Spherically inhomogeneous fluids. I. Percus–Yevick hard spheres: Osmotic coefficients and triplet correlations

Phil Attard

Citation: J. Chem. Phys. **91**, 3072 (1989); doi: 10.1063/1.456930
View online: http://dx.doi.org/10.1063/1.456930
View Table of Contents: http://jcp.aip.org/resource/1/JCPSA6/v91/i5
Published by the American Institute of Physics.

Spherically inhomogeneous fluids. I. Percus–Yevick hard spheres: Osmotic coefficients and triplet correlations

Phil Attard[a)]
Centre de Recherche Paul Pascal, Domaine Universitaire, Talence 33405 Cedex, France

(Received 20 December 1988; accepted 20 April 1989)

For fluids in a spherically symmetric external field, it is shown that the Ornstein–Zernike convolution integral becomes a simple algebraic equation upon Legendre transformation. Applying the usual closure relations, the full inhomogeneous pair correlation functions become available. A discrete orthogonal transform pair is also derived, which, in conjunction with the Legendre factorization, makes computations feasable for these generic systems. The general method is here applied to a bulk uniform fluid of hard spheres, using the pair Percus–Yevick closure, but at the triplet level in the hierarchy of distribution functions. Consequently, the pair distribution function and the osmotic coefficient are better than the known analytic results. The method enables the accurate calculation of the triplet correlation function, and several examples are given.

I. INTRODUCTION

The properties of bulk fluids are well understood at the two-particle level. A popular and routine procedure is based on the Ornstein–Zernike equation, closed with some approximate relation between the correlation functions. Only recently have inhomogeneous fluids in planar geometry been described at a similar level.[1–8] That the Ornstein–Zernike convolution integral factors in three- or two-dimensional Fourier space makes the bulk and planar systems the only two geometries in which computations are presently feasable. It is the purpose of this paper to present a transformation which factors the Ornstein–Zernike equation in spherical geometry.

The properties of a fluid in the vicinity of an isolated spherically symmetric external field may hence be described accurately. Examples include the liquid–vapor interface about a drop or cavity, and a simple fluid near to a large spherical particle. The Hamiltonian which specifies the system need only depend on positions of pairs of fluid particles via the two radial coordinates and the mutual angle. Thus, image interactions may be included in describing the electric double layer around a micelle, vesicle, macroion or charged colloid. The inhomogeneous (anisotropic, translationally variant) pair correlations can be calculated explicitly. The results obtained by this method are at the two-particle level, and should be distinguished from the essentially singlet approaches which use integral equations for a bulk mixture, even though the components be highly asymmetric in size, charge, or concentration. While the procedure introduced here applies with full accuracy only to an isolated inhomogeneity, it may prove possible (by perturbation, superposition or cell approximations) to use it to describe an asymmetric mixture at finite concentrations, or to evaluate the effective interaction between two spherical particles.

A particularly interesting possibility is to consider the spherical inhomogeneity to be itself a particle of the fluid (which must be specified by spherically symmetric pair potentials). The consequent inhomogeneous density profile corresponds to the pair distribution function of the bulk fluid, and the inhomogeneous pair correlations in the presence of the fixed particle are simply related to the triplet correlation functions of the uniform fluid. The latter quantities have been studied experimentally,[9,10] by simulation,[10–13] and in various theoretical approximations.[14–18] Besides intrinsic interest, triplet correlation functions for bulk fluids can improve density functional theories for inhomogeneous fluids, or for freezing transitions (Ref. 18, for example,). They may also be used in evaluating thermodynamic quantities of the fluid. Because one is using an approximate closure at a higher level in the hierarchy than is usual, one would expect the pair distribution and other quantities to be consequently more accurate, as will indeed be demonstrated here.

This paper is divided into two parts. In the following section the spherically inhomogeneous fluid problem is formulated. It is shown that the Ornstein–Zernike equation is transformed to an algebraic equation in Legendre space, and a discrete orthogonal transform pair is given. These render feasable the computations in the general case. Examples of closures for the inhomogeneous correlation functions, and equations to determine the density profile are given in spherical geometry. The second part deals specifically with hard-spheres and the Percus–Yevick closure. The Treizenberg–Zwanzwig equation for the profile is applied to this fluid with a hard-sphere inhomogeneity. Results are presented for the osmotic coefficient, the compressibility, and the radial and the triplet distribution functions of a bulk uniform hard-sphere fluid. Details of the numerical procedures are relegated to the Appendix.

II. SPHERICALLY INHOMOGENEOUS SYSTEMS

A. Factorization of the Ornstein–Zernike equation

Consider a classical fluid in which the Hamiltonian consists only of one- and two-body terms. A spherically inhomogeneous system is one in which the external potential $V(r)$ depends only on the distance from the origin $r = |\mathbf{r}|$, and the

[a)] Present address: Department of Chemistry, University of British Columbia, Vancouver, British Columbia V6T1Y6, Canada.

 0021-9606/89/173072-11$02.10

pair potential $u(r_1, r_2, \theta_{12})$ depends on the particles' radial coordinates and mutual angle. This contains spherically symmetric pair potentials (such as hard sphere, Lennard-Jones or Coulomb) but is, in fact, more general (e.g., electrostatic images can be included). The inhomogeneous one- and two-particle distribution functions exhibit the same symmetries as the Hamiltonian, and the Ornstein-Zernike equation is

$$h(r_1,r_2,\theta_{12}) = c(r_1,r_2,\theta_{12}) + \int d\mathbf{r}_3 c(r_1,r_3,\theta_{13})\rho(r_3)h(r_3,r_2,\theta_{32}), \tag{1}$$

where $h \equiv g - 1$ is the total correlation function, g is the radial distribution function, c is the direct correlation function, and ρ is the singlet density profile. The volume element in spherical coordinates is $d\mathbf{r} = r^2 \sin\theta dr\, d\theta\, d\phi$. Without loss of generality, take $\theta_1 = \phi_1 = \phi_2 = 0$ and one has the geometrical relation

$$\cos\theta_{32} = \cos\theta_2 \cos\theta_3 + \sin\theta_2 \sin\theta_3 \cos\phi_3. \tag{2}$$

Hereinafter use the notation

$$x \equiv \cos\theta. \tag{3}$$

It follows that the Ornstein–Zernike equation may be written

$$y(r_1,r_2,x_2) = \int_0^\infty dr_3\, r_3^2\, \rho(r_3) \int_0^{2\pi} d\phi_3 \times \int_{-1}^{1} dx_3\, c(r_1,r_3,x_3)h(r_3,r_2,x_{32}), \tag{4}$$

where $y \equiv h - c$ is a continuous function, even across hard core discontinuities.

Now define the continuous Legendre transform as

$$f(x) = \sum_{n=0}^{\infty} \hat{f}_n P_n(x), \tag{5}$$

where $P_n(x)$ is the Legendre polynomial of degree n. The expansion coefficients are given by

$$\hat{f}_n = \frac{2n+1}{2} \int_{-1}^{1} dx\, f(x) P_n(x) \tag{6}$$

which follows since the Legendre polynomials satisfy the orthogonality relation

$$\int_{-1}^{1} dx\, P_n(x) P_m(x) = \frac{2}{2n+1} \delta_{n,m}, \tag{7}$$

$\delta_{n,m}$ being the Kronecker delta. Taking the Legendre transform of Eq. (4) one achieves (temporarily suppressing the radial dependence for brevity)

$$\begin{aligned}\hat{y}_n &= \frac{2n+1}{2} \int_{-1}^{1} dx_2 \int_0^{2\pi} d\phi_3 \times \int_{-1}^{1} dx_3\, P_n(x_2) c(x_3) h(x_{32}) \\ &= \frac{2n+1}{2} \sum_{i,j=0}^{\infty} \hat{c}_i \hat{h}_j \int_{-1}^{1} dx_2 \int_0^{2\pi} d\phi_3 \times \int_{-1}^{1} dx_3\, P_n(x_2) P_i(x_3) P_j(x_{32}).\end{aligned} \tag{8}$$

Now the well-known (Ref. 19, for example) addition theorem for spherical harmonics is [with x_{32} having the form of Eq. (2)]

$$P_j(x_{32}) = P_j(x_3)P_j(x_2) + 2 \sum_{m=1}^{j} \frac{(j-m)!}{(j+m)!} P_j^m(x_3) P_j^m(x_2) \cos(m\phi_3). \tag{9}$$

When inserted in Eq. (8), the sum of associated Legendre polynomials vanishes because of the integration of the cosines over the interval $[0,2\pi]$. Then twice using the orthogonality relation (7) for the remaining product of Legendre polynomials, one achieves the desired factorisation

$$\hat{y}_n = \frac{4\pi}{2n+1} \hat{c}_n \hat{h}_n. \tag{10}$$

Explicity writing the radial dependence in full, one has

$$\hat{y}_n(r_1,r_2) = \frac{4\pi}{2n+1} \int_0^\infty dr_3\, r_3^2 \hat{c}_n(r_1,r_3)\rho(r_3)\hat{h}_n(r_3,r_2). \tag{11}$$

The one-dimensional convolution integral that remains in the final expression also occurs in the planar inhomogeneous problem.[1–8] It is this remaining convolution which makes inhomogeneous problems computationally more demanding than bulk problems, but not impossibly so. Since the fluid attains bulk properties far from the inhomogeneity, the upper limit of the integral can be made finite, as is discussed in more detail in the Appendix.

B. Discrete, orthogonal transform

In practice one cannot compute with the continuous Legendre transform pair Eqs. (5) and (6) directly; a discrete N-point version is required. This is

$$\hat{f}_n = \frac{2n+1}{2} \sum_{i=1}^{N} w_i f_i P_n(x_i), \tag{12}$$

$$f_i = \sum_{n=0}^{N-1} \hat{f}_n P_n(x_i), \tag{13}$$

where $f_i \equiv f(x_i)$, the nodes $\{x_i\}_{i=1}^N$ are the zeros of $P_N(x)$ and

$$w_i = \frac{2}{1-x_i^2} [P'_N(x_i)]^{-2} \tag{14}$$

are the weights associated with the Gauss–Legendre quadrature (see Sec. 25.4 of Ref. 20). This quadrature is *exact* for any polynomial of degree $\leqslant 2N-1$. In particular, the orthogonality relation (7) is preserved

$$\sum_{i=1}^{N} w_i P_n(x_i) P_m(x_i) = \frac{2}{2n+1} \delta_{n,m}, \tag{15}$$

since $0 \leqslant n, m \leqslant N-1$. One can also explicitly show that the observe holds namely

$$\sum_{n=0}^{N-1} \frac{2n+1}{2} P_n(x_i) P_n(x_j) = \frac{1}{w_i} \delta_{i,j}, \tag{16}$$

using the fact that $P_N(x_i) = P_N(x_j) = 0$. This formula, which expresses the completeness of the expansion, can also be obtained from the Christoffel-Darboux lemma (see Sec. 22.12 of Ref. 20). These two results mean that Eqs. (12) and

(13) form a discrete, orthogonal transform pair, a very great advantage in any iterative numerical work. Any other choice to discretise the continuous Legendre transform [e.g., evaluating Eq. (6) by Simpson's rule] would yield only approximate orthogonality.

C. Closure and profile relations

The Ornstein–Zernike equation contains three unknown functions–the density, and the inhomogeneous direct and total correlation functions; two more equations are required. There are several approximate closures relating the correlation functions which do not depend on translational invariance and can hence be applied directly to the inhomogeneous problem. Two common examples are the Percus–Yevick

$$c(r_1,r_2,x_{12}) = g(r_1,r_2,x_{12})\{1 - \exp[\beta u(r_1,r_2,x_{12})]\}, \tag{17}$$

and the hypernetted chain

$$h(r_1,r_2,x_{12}) = \exp[h(r_1,r_2,x_{12}) - c(r_1,r_2,x_{12}) - \beta u(r_1,r_2,x_{12})] - 1. \tag{18}$$

Here $\beta = (k_B T)^{-1}$ is the inverse temperature, and u is the pair potential.

Several exact equations relate the density profile to the external field V. One due to Triezenberg and Zwanzwig[21] involves the total correlation function:

$$\nabla\rho(\mathbf{r}_1) = -\beta\rho(\mathbf{r}_1)\nabla V(\mathbf{r}_1) - \beta\rho(\mathbf{r}_1)\int d\mathbf{r}_2\,\rho(\mathbf{r}_2)h(\mathbf{r}_1,\mathbf{r}_2)\nabla V(\mathbf{r}_2).$$

For spherically inhomogeneous systems it reads

$$\begin{aligned}\rho'(r_1) &= -\beta\rho(r_1)V'(r_1) - 2\pi\beta\rho(r_1)\int_{-1}^{1} dx \times\int_0^\infty dr_2\, r_2^2\,\rho(r_2)h(r_1,r_2,x)xV'(r_2)\\ &= -\beta\rho(r_1)V'(r_1) - \frac{4\pi\beta\rho(r_1)}{3}\times\int_0^\infty dr_2\, r_2^2\,\rho(r_2)\hat{h}_1(r_1,r_2,)V'(r_2),\end{aligned} \tag{19}$$

where the prime denotes differentiation with respect to argument. Another[22,23] uses instead the direct correlation function

$$\nabla\rho(\mathbf{r}_1) = -\beta\rho(\mathbf{r}_1)\nabla V(\mathbf{r}_1) + \rho(\mathbf{r}_1)\int d\mathbf{r}_2\, c(\mathbf{r}_1,\mathbf{r}_2)\nabla\rho(\mathbf{r}_2)$$

and it is written in the present geometry as

$$\rho'(r_1) = -\beta\rho(r_1)V'(r_1) + \frac{4\pi\beta\rho(r_1)}{3}\int_0^\infty dr_2\, r_2^2\,\hat{c}_1(r_1,r_2,)\rho'(r_2). \tag{20}$$

The first member of the Yvon–Born–Green hierarchy[24–26] is also suitable. It involves the radial distribution function and pair potential:

$$\nabla\rho(\mathbf{r}_1) = -\beta\rho(\mathbf{r}_1)\nabla V(\mathbf{r}_1) - \beta\rho(\mathbf{r}_1)\int d\mathbf{r}_2\, g(\mathbf{r}_1,\mathbf{r}_2)\nabla_{\mathbf{r}_1} u(\mathbf{r}_1,\mathbf{r}_2).$$

The form applicable in spherical symmetry is

$$\begin{aligned}\rho'(r_1) &= -\beta\rho(r_1)V'(r_1) - 2\pi\beta\rho(r_1)\int_{-1}^{1} dx \times\int_0^\infty dr_2\, r_2^2\, g(r_1,r_2,x)\frac{du(r_1,r_2,x)}{dr_1}\\ &= -\beta\rho(r_1)V'(r_1) - 2\pi\beta\rho(r_1)\sum_n \frac{2}{2n+1}\times\int_0^\infty dr_2\, r_2^2\,\hat{g}_n(r_1,r_2)\frac{d\hat{u}_n(r_1,r_2)}{dr_1}.\end{aligned} \tag{21}$$

Any one of these three equations may be used to determine the density profile. The boundary condition is that the profile should equal the bulk density at large r.

Note that the closures constitute an approximation, as in the bulk case, whereas the Ornstein–Zernike equation and the equations for the profile are exact. However, the closure is the *only* approximation introduced (besides those necessary for the numerical solution of the problem) and hence the inhomogeneous problem can be solved with an accuracy comparable to that usually achieved in bulk. In fact, for the case when the spherical inhomogeneity is a particle of the fluid, the closure is applied at the triplet level, one step higher in the hierarchy of distribution functions. Hence one expects better results for this problem than the usual bulk formulation.

III. PERCUS-YEVICK HARD SPHERES, BULK

A. Hamiltonian, profile, and closure

The general method derived above will now be illustrated by application to a hard-sphere fluid. This fluid is a suitable test case, being both well defined and extensively studied. The results give some information on the accuracy of the procedure, and hopefully provide new perspectives into the behaviour of the correlation functions. The actual data obtained may be applied to other fluids using the hard-sphere fluid as a reference.

Atoms of a hard-sphere fluid interact with a pair potential

$$u(r_1,r_2,x_{12}) = \begin{cases}\infty, & r_{12} < d\\ 0, & r_{12} > d\end{cases}, \tag{22}$$

where $r_{12} = \sqrt{r_1^2 + r_2^2 - 2r_1r_2x_{12}}$ is the distance between the atoms and d is the hard-sphere diameter. Now consider a hard-sphere particle of diameter D and fixed at the origin. This causes an external potential

$$V(r) = \begin{cases}\infty, & r < S\\ 0, & r > S\end{cases}, \tag{23}$$

where $S = (d + D)/2$. At this time in the analysis take $D \neq d$. However, when $D = d$, the case for which detailed results will be presented below, the fixed particle is just one of the atom of the fluid.

Of the equations for the profile, the one due to Triezen-

berg and Zwanzwig[21] was found convenient. First define the continuous density function

$$\rho_c(r) \equiv \rho(r) e^{\beta V(r)},$$

and note that

$$\beta V'(r) e^{-\beta V(r)} = \frac{d}{dr}(1 - e^{-\beta V(r)}) = -\delta(r - S),$$

where $\delta(r)$ is the Dirac delta. Then for the present problem Eq. (19) becomes

$$\rho'(r) = \rho_c(r)\delta(r - S) + (4\pi/3)\rho(r)\rho_c(S)S^2\hat{h}_1(r,S). \tag{24}$$

This may be integrated to yield $(r > S)$

$$\rho(r) = \rho(R) + (4\pi/3)\rho_c(S)S^2 \int_R^r dr'\, \rho(r')\hat{h}_1(r',S), \tag{25}$$

where $\rho_c(S) = \rho(S^+)$ is the contact density, and R is some large radius (several hard-sphere diameters) after which bulk properties are assumed.

For a hard-sphere fluid the Percus–Yevick (PY) closure Eq. (17) becomes

$$c(r_1,r_2,x_{12}) = 0, \quad r_{12} > d, \tag{26}$$

which is supplemented with the exact result

$$g(r_1,r_2,x_{12}) = 0, \quad r_{12} < d. \tag{27}$$

This is the closure to be used for the present problem since it works well for a bulk hard-sphere fluid where an analytic solution exists.[27,28] It has also been successfully applied to the planar inhomogeneous hard-sphere system.[1,29–31]

B. Osmotic coefficient and compressibility

Results will now be presented for a bulk uniform fluid of hard-spheres, i.e., $D = S = d$. Since in this case the method corresponds to using the closure at the triplet level, we shall designate our results "PY3" to distinguish them from the analytic solution[27,28] of the PY closure for the bulk pair correlation ("PY2").

The osmotic coefficient is related to the pressure by

$$\phi = \frac{P}{\rho k_B T}, \tag{28}$$

where ρ without argument denotes the bulk density. For hard spheres the virial equation is

$$\phi_v = 1 + 4\eta g(d^+), \tag{29}$$

where the packing fraction

$$\eta \equiv (\pi/6)\rho d^3 \tag{30}$$

is the only parameter required to specify the hard-sphere fluid nontrivially. In the spherical system when the inhomogeneity is an atom of the fluid, the one-particle distribution (the density profile) corresponds to the pair distribution function of the bulk. Hence, the value of the bulk radial distribution function at contact is here

$$g(d^+) = \rho_0(d^+)/\rho, \tag{31}$$

where the subscript indicates that the singlet profile is about an atom fixed at the origin.

One can also calculate the osmotic coefficient via the compressibility relation

$$\phi_c = \frac{1}{\rho}\int_0^\rho \frac{d\rho'}{\rho' k_B T \kappa_T}, \tag{32}$$

where the isothermal compressibility κ_T is given by

$$\rho k_B T \kappa_T = [1 + \rho\tilde{h}(0)] \equiv 1 + \rho \int d\mathbf{r}\, h(r). \tag{33}$$

In an exact theory the two thermodynamic paths to the osmotic coefficient should agree; the consistency of this quantity provides some measure by which to judge the accuracy of an approximate theory. For example, the analytic solution to the PY closure yields for the virial

$$\phi_v^{PY2} = \frac{1 + 2\eta + 3\eta^2}{(1 - \eta)^2} \tag{34}$$

and for the compressibility

$$\phi_c^{PY2} = \frac{1 + \eta + \eta^2}{(1 - \eta)^3}. \tag{35}$$

The Carnahan–Starling (CS) equation of state,[33] a linear combination of these two results which is nearly exact over the whole density regime, is

$$\phi^{CS} = \frac{1 + \eta + \eta^2 - \eta^3}{(1 - \eta)^3}. \tag{36}$$

Table I compares the osmotic coefficient given by the various theories with Monte Carlo (MC)[34] and molecular dynamics (MD)[35] results. The simulations were performed with 108 atoms and so the error due to finite size effects is of the order of 1%. It is manifest that the PY3 virial performs better than the PY2, being in closer agreement with the simulations. Indeed, it is comparable in accuracy to the CS approximation up to quite high packing fractions. The PY3 virial and compressability results are also more consistent than the PY2. For example at $\rho d^3 = 0.5$, the discrepancy between the two routes is 2% for PY3 and 4% for PY2. The virial and compressability routes bracket the real pressure, with the former being an upper bound in PY3, in contrast to PY2. At higher densities the finite size of the mesh begins to effect the PY3 results, causing the calculated virial osmotic coefficient to be underestimated.

The compressibility osmotic coefficient is less reliable at higher densities. The radial distribution function decays more slowly at higher couplings, and it becomes exceedingly difficult to calculate the isothermal compressibility with numerical accuracy. This is evident from the data in Table II, and is the reason that values for κ_T are not usually available in numerical schemes. The error in ϕ_c (and ϕ_v) at higher densities probably reflects computational limitations, rather than the error intrinsic to the PY3 approximation.

The fundamental reason that PY3 perfoms better than PY2 is because the approximate closure is used at a higher level in the hierarchy of distribution functions. The link between the triplet and pair levels is the exact profile relationship. The computations are more demanding than the usual bulk numerical procedures (in general), and much more so than the analytic results available for this case in particular. The improved thermodynamics *per se* would not ordinarily justify the application of the present theory to bulk problems. However, examples of accurate triplet correlations will now be presented, and since these are not readily

TABLE I. Osmotic coefficients: virial (ϕ_v), and compressability (ϕ_c, in parenthesis).

ρd^3	MC[a]	PY3	PY2	CS	ρd^3	MC[a]	PY3	PY2	CS
0.20	1.561	1.554 (1.555)	1.550 (1.555)	1.553	0.70	5.629 5.89[b]	5.722	5.323 (5.904)	5.710
0.30	1.972	1.969 (1.970)	1.954 (1.973)	1.967	0.75	6.533	6.59	6.095 (6.906)	6.636
0.40	2.517	2.525 (2.511)	2.481 (2.537)	2.518	0.80	7.654	7.70	7.001 (8.124)	7.750
0.50	3.216	3.279 (3.216)	3.173 (3.307)	3.262	0.83	8.60[b]	8.4	7.660 (9.039)	8.579
0.60	4.219	4.312 (4.188)	4.091 (4.380)	4.283	0.85	8.951	8.6	8.067 (9.615)	9.099
0.65	4.896	4.962 (4.954)	4.661 (5.073)	4.935	0.88	10.2[b]	9.6	8.900 (10.818)	10.179

[a] Reference 34.
[b] Reference 35.

available by other methods, they do provide motivation for exploring the bulk in this fashion.

C. Pair and triplet distribution functions

Figure 1 displays a comparison of the bulk radial distribution function given by the MC, PY2, and PY3 approximations. In the latter approach $g(r) \equiv \rho_0(r)/\rho$, and these data follow the pronounced oscillations of the function quite accurately, and somewhat better than PY2. The last were computed by fast Fourier inversion of the analytic expressions.[27,28] Lengths here and below are in units of the hard-sphere diameter d. Values of $g(r)$ are tabulated in Table III on a coarse grid in the x–y plane. Direct comparison between PY3 and PY2 is possible from the values below and above the diagonal respectively. For example, at $r = 1.03$ PY3 gives $g(r) = 2.863$ at the point (0.25, 1.0), and PY2 gives 2.697 (1.0, 0.25).

The inhomogeneous pair correlation function calculated in the PY3 scheme $g_0(\mathbf{r}_1,\mathbf{r}_2)$, gives, when multiplied by ρ, the probability of finding an atom at $\mathbf{r}_2$, given atoms fixed at $\mathbf{r}_1$ and the origin, Hence it is simply related to the bulk triplet correlation function by

$$g(0,\mathbf{r}_1,\mathbf{r}_2) \equiv g(r_1)g(r_2)g_0(\mathbf{r}_1,\mathbf{r}_2). \tag{37}$$

The triplet distribution function approaches unity only when all of the trio are far apart. Examples are given in Figs. 2. Each perspective has the second atom a fixed distance from the central atom, with a point in the plane corresponding to the position of the third atom. The plots may also be interpreted as the singlet profile about two fixed atoms $\rho g_{0,\mathbf{r}_1}(\mathbf{r}_2)$, in which case the maxima correspond to 6.1ρ, 8.8ρ, and to 3.1ρ for $r_1 = 1$, 2, and 3, respectively. When the first two atoms are in contact, the fluid is highly structure showing oscilatory behaviour extending far from the particles. Here there is a sharp peak in the fluid in the two small wedges that remain between the spheres in contact [two grid points in Fig. 2(a)]. As the two atoms separate, the height of the oscillations generally decrease (note the change in scale between each figure). There is an enhancement of the profile between the two atoms at a separation of two hard sphere diameters, and a marked depletion at three. Hence if one tried to describe the interaction between two spheres by considering the singlet profile *only* in the region between them, one would erroneously predict a period of $\approx 2d$ for the oscillation in the effective potential. This simple example indicates that care is needed when evaluating the effective interaction between two particles, and one should consider the whole structure of the fluid, not only the density at the midpoint between the particles.

TABLE II. Isothermal compressability, $\rho k_B T \kappa_T$.

ρd^3	PY3	PY2
0.10	0.6605	0.6608
0.20	0.4394	0.4392
0.30	0.2949	0.2923
0.40	0.2013	0.1940
0.50	0.1375	0.1279
0.60	0.0852	0.0834
0.65	0.0588	0.0670
0.70	0.0925	0.0536
0.75	0.0024	0.0427

The Kirkwood superposition approximation[14] consists in approximating the inhomogeneous pair correlation everywhere by its bulk form,

$$g_0(\mathbf{r}_1,\mathbf{r}_2) \approx g(r_{12}). \tag{38}$$

This approximation is exact asymptotically, when any one of

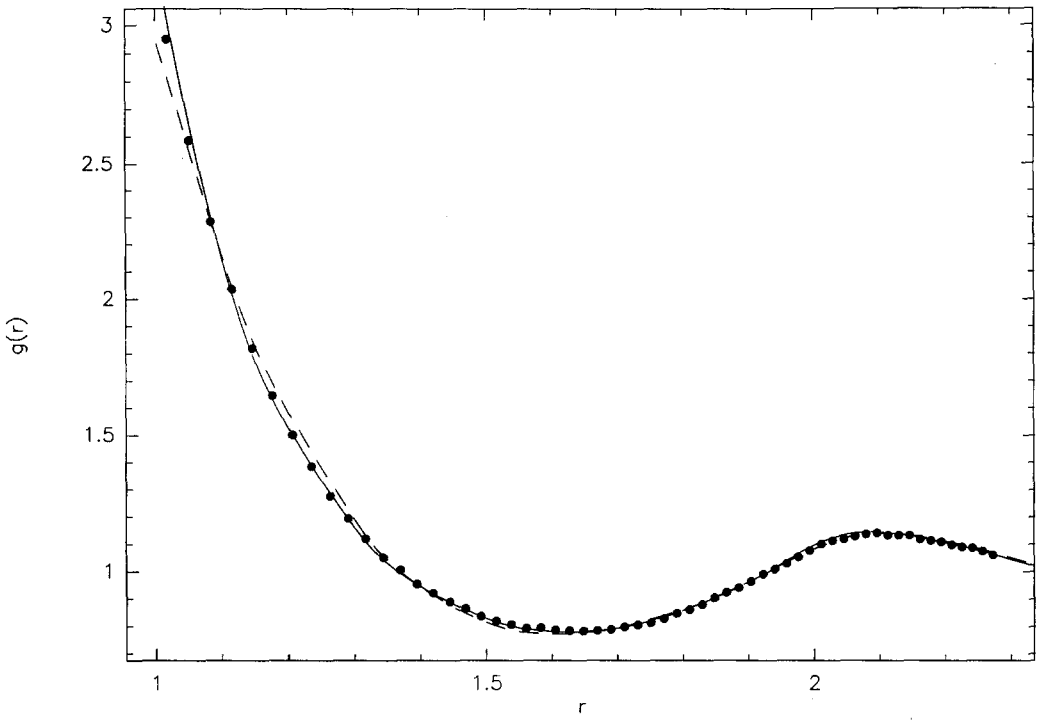

FIG. 1. Radial distribution function $g(r)$ as given by PY3 (solid line) and PY2 (dashed line) at $\rho d^3 = 0.7$. The dots are MC data from Ref. 34.

the three atoms is far separated from the others. There have been several tests of the validity of this approach,[11–13] and it would be fair to conclude that it is quite reasonable, the notable exception being when it is used to close the BGY hierarchy.

To test the accuracy of the PY3 triplet distribution function, one can compare it (indirectly) to the MD data. Alder[11] has examined $R(r)$, the ratio of the triplet function to its superposition approximation for equilateral triangle configurations of side r. At densities $\rho d^3 = 0.471$, 0.707, and 0.832, for $r = 1.13$, 1.08, and 1.05, he finds $R(r) = 0.91$, 0.86, and 0.88 respectively. The PY3 procedure gives 0.95, 0.85, and 0.80. MD and PY3 data for isoceles triangles at the higher density $\rho d^3 = 0.884$ are in reasonable agreement, both showing the same trends, but the PY3 data being consistently $\approx 10\%$ below the MD results. The size of the mesh used in the PY3 calculations is probably manifest here. These limited comparisons do not completely establish the accuracy of the PY3 triplet distribution functions. However, one can conclude that there is no reason to believe that they are in greater error than are the PY2 bulk pair distribution functions.

A direct and extensive test of the superposition approximation can be made from the data in Tables IV–VI. These

TABLE III. Radial distribution function $g(r)$ $\mathbf{r} = x\mathbf{i} + y\mathbf{j}$: PY3 (on and below) and PY2 (above) the diagonal $x = y$, for $\rho d^3 = 0.7$.

	0.00	0.25	0.50	0.75	1.00	1.25	1.50	1.75	2.00	2.25	2.50
0.00	0.000	0.000	0.000	0.000	2.949	1.375	0.819	0.825	1.082	1.082	0.958
0.25	0.000	0.000	0.000	0.000	2.697	1.279	0.802	0.838	1.095	1.074	0.955
0.50	0.000	0.000	0.000	0.000	2.055	1.064	0.778	0.881	1.132	1.048	0.949
0.75	0.000	0.000	0.000	2.515	1.375	0.859	0.787	0.966	1.137	1.009	0.945
1.00	3.221	2.863	2.030	1.329	0.927	0.773	0.865	1.095	1.091	0.969	0.952
1.25	1.329	1.240	1.050	0.870	0.782	0.835	1.023	1.132	1.017	0.947	0.973
1.50	0.832	0.816	0.789	0.788	0.861	1.027	1.139	1.048	0.958	0.954	1.003
1.75	0.822	0.835	0.879	0.967	1.107	1.130	1.042	0.965	0.948	0.987	1.027
2.00	1.096	1.107	1.140	1.137	1.084	1.012	0.959	0.949	0.982	1.022	1.024
2.25	1.075	1.067	1.042	1.006	0.968	0.948	0.955	0.988	1.023	1.025	1.003
2.50	0.959	0.956	0.950	0.946	0.953	0.973	1.004	1.027	1.023	1.002	0.987
2.75	0.963	0.966	0.973	0.988	1.007	1.024	1.029	1.016	0.997	0.987	0.990
3.00	1.022	1.023	1.026	1.029	1.027	1.017	1.003	0.991	0.986	0.991	1.001
3.25	1.017	1.016	1.012	1.006	0.997	0.990	0.986	0.988	0.996	1.004	1.007
3.50	0.989	0.989	0.987	0.986	0.987	0.990	0.995	1.002	1.007	1.007	1.002
3.75	0.991	0.992	0.994	0.996	1.000	1.004	1.007	1.007	1.004	1.000	0.997
4.00	1.006	1.006	1.007	1.007	1.007	1.006	1.003	1.000	0.997	0.996	0.997
4.25	1.004	1.004	1.003	1.002	1.000	0.998	0.997	0.996	0.997	0.999	1.001
4.50	0.997	0.997	0.997	0.996	0.996	0.997	0.998	0.999	1.001	1.002	1.002
4.75	0.998	0.998	0.998	0.999	1.000	1.001	1.002	1.002	1.002	1.001	1.000
5.00	1.002	1.002	1.002	1.002	1.002	1.002	1.001	1.001	1.000	0.999	0.999

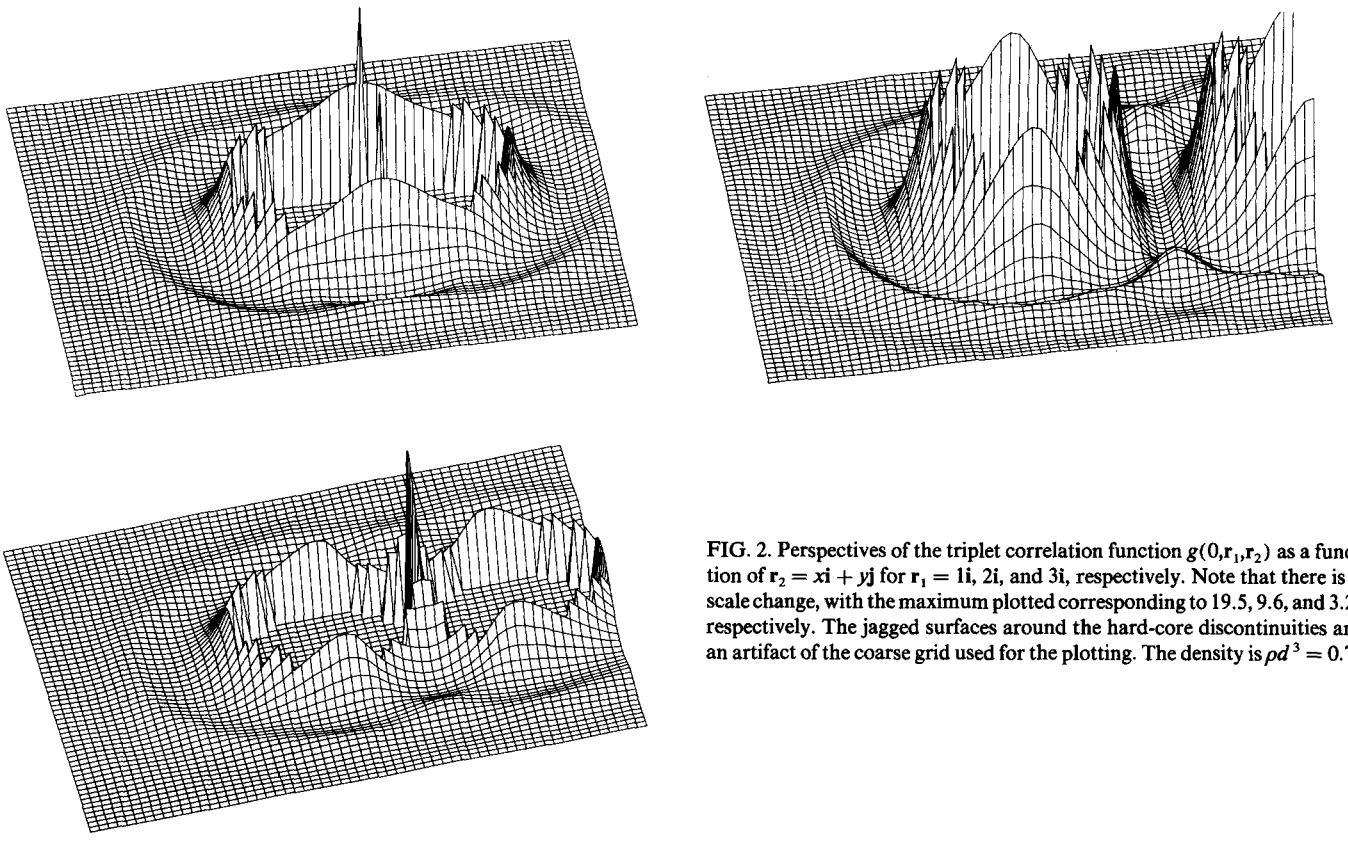

FIG. 2. Perspectives of the triplet correlation function $g(0,\mathbf{r}_1,\mathbf{r}_2)$ as a function of $\mathbf{r}_2 = x\mathbf{i} + y\mathbf{j}$ for $\mathbf{r}_1 = 1\mathbf{i}$, $2\mathbf{i}$, and $3\mathbf{i}$, respectively. Note that there is a scale change, with the maximum plotted corresponding to 19.5, 9.6, and 3.2, respectively. The jagged surfaces around the hard-core discontinuities are an artifact of the coarse grid used for the plotting. The density is $\rho d^3 = 0.7$.

contains $g_0(\mathbf{r}_1,\mathbf{r}_2)$ on the same mesh as $g(\mathbf{r})$ in Table III. Thus, the point (0.5, 2.0) of Table IV, which corresponds to $g_0(1\mathbf{j}, 0.5\mathbf{i} + 2.0\mathbf{j}) = 1.78$, should be compared with the corresponding values of $g(r_{12})$ from Table III: 2.03 (0.5, 1.0) for PY3 or 2.06 (1.0, 0.5) for PY2. Superposition is clearly valid at larger separations. When the two particles are separated by three hard-sphere diameters, Table VI, the anisotropic pair correlation is 0.950 at (2.0, 4.75), to be compared with 0.949 (1.75, 2.0) and 0.948 (2.0, 1.75) for PY3 and PY2, respectively.

Figure 3 gives the PY3 radial distribution function $g(r)$ at the densities $\rho d^3 = 0.5$, and $\rho d^3 = 0.8$. These are compared to the triplet correlation function $g(0,\mathbf{r}_1,\mathbf{r}_2)$ for isoceles triangle configurations, $(r_1 = r_2 = s, r_{12} = r)$, divided by $g(s)^2$. This ratio [which is just $g_0(\mathbf{r}_1,\mathbf{r}_2)$] approaches $g(r)$ for large s or large r, as is to be expected from the asymptotic

TABLE IV. Inhomogeneous pair correlation function $g_0(\mathbf{r}_1\mathbf{r}_2)$, as a function of $\mathbf{r}_2 = (x,y)$, with one sphere fixed at the region (0,0) and the second ar $\mathbf{r}_1 = (0,1)$, and $\rho d^3 = 0.7$.

	0.00	0.25	0.50	0.75	1.00	1.25	1.50	1.75	2.00	2.25	2.50
0.00	···	···	···	···	0.885	0.903	0.873	1.064	1.063	0.989	0.959
0.25	···	···	···	···	1.154	0.946	0.808	0.901	1.109	1.023	0.955
0.50	···	···	···	···	1.736	1.094	0.810	0.814	1.103	1.058	0.960
0.75	···	···	···	0.000	2.485	1.348	0.837	0.778	1.080	1.085	0.965
1.00	0.000	0.000	0.000	0.000	3.074	1.535	0.844	0.790	1.075	1.098	0.965
1.25	0.000	0.000	0.000	0.000	3.116	1.470	0.808	0.821	1.101	1.092	0.955
1.50	0.000	0.000	0.000	0.000	2.425	1.115	0.733	0.877	1.144	1.065	0.942
1.75	0.000	0.000	0.000	2.591	1.289	0.784	0.762	0.980	1.159	1.015	0.936
2.00	2.710	2.451	1.783	1.165	0.835	0.760	0.878	1.126	1.107	0.962	0.945
2.25	1.244	1.165	0.994	0.836	0.795	0.873	1.060	1.150	1.008	0.936	0.973
2.50	0.863	0.848	0.820	0.837	0.919	1.061	1.145	1.030	0.942	0.952	1.009
2.75	0.856	0.854	0.900	0.990	1.110	1.112	1.018	0.948	0.947	0.994	1.032
3.00	1.079	1.089	1.109	1.104	1.056	0.990	0.948	0.952	0.991	1.029	1.024
3.25	1.060	1.052	1.030	0.996	0.964	0.952	0.966	0.999	1.029	1.025	0.998
3.50	0.971	0.969	0.962	0.960	0.966	0.986	1.012	1.029	1.020	0.997	0.985
3.75	0.972	0.974	0.980	0.993	1.009	1.023	1.024	1.010	0.993	0.985	0.991
4.00	1.015	1.016	1.019	1.022	1.020	1.011	0.998	0.989	0.987	0.994	1.004
4.25	1.013	1.012	1.009	1.003	0.996	0.991	0.988	0.991	0.999	1.006	1.007
4.50	0.993	0.992	0.991	0.990	0.990	0.993	0.998	1.004	1.007	1.006	1.001
4.75	0.994	0.994	0.996	0.998	1.001	1.004	1.006	1.006	1.002	0.999	0.996
5.00	1.004	1.004	1.005	1.005	1.005	1.004	1.002	0.999	0.997	0.997	0.998

TABLE V. Same as Table IV but with $\mathbf{r}_1 = (0,2)$.

	0.00	0.25	0.50	0.75	1.00	1.25	1.50	1.75	2.00	2.25	2.50
0.00	...	...	...	...	0.995	1.063	0.964	0.937	0.955	1.035	1.027
0.25	...	...	...	...	1.015	1.185	1.052	0.960	0.926	1.004	1.036
0.50	...	...	...	...	0.839	1.049	1.164	1.036	0.935	0.969	1.014
0.75	...	...	...	0.826	0.780	0.824	1.086	1.128	0.987	0.954	0.982
1.00	2.710	2.483	1.943	1.354	0.896	0.769	0.931	1.092	1.065	0.970	0.960
1.25	0.000	0.000	0.000	2.389	1.326	0.859	0.833	0.965	1.109	1.112	0.955
1.50	0.000	0.000	0.000	0.000	1.979	1.072	0.806	0.874	1.111	1.057	0.959
1.75	0.000	0.000	0.000	0.000	2.624	1.300	0.824	0.831	1.080	1.084	0.964
2.00	0.000	0.000	0.000	0.000	2.957	1.396	0.836	0.812	1.066	1.088	0.963
2.25	0.000	0.000	0.000	0.000	2.749	1.297	0.805	0.822	1.085	1.075	0.958
2.50	0.000	0.000	0.000	0.000	2.115	1.068	0.772	0.876	1.124	1.050	0.949
2.75	0.000	0.000	0.000	2.492	1.379	0.864	0.789	0.973	1.136	1.012	0.946
3.00	2.816	2.604	1.995	1.337	0.918	0.780	0.877	1.094	1.091	0.970	0.952
3.25	1.309	1.229	1.034	0.842	0.775	0.847	1.031	1.127	1.014	0.945	0.974
3.50	0.826	0.812	0.780	0.792	0.877	1.031	1.137	1.044	0.957	0.955	1.005
3.75	0.837	0.845	0.885	0.977	1.102	1.127	1.043	0.963	0.950	0.990	1.026
4.00	1.101	1.111	1.133	1.134	1.085	1.011	0.956	0.950	0.984	1.023	1.023
4.25	1.071	1.064	1.039	1.003	0.966	0.946	0.956	0.990	1.022	1.025	1.002
4.50	0.958	0.956	0.949	0.947	0.954	0.975	1.005	1.027	1.023	1.002	0.987
4.75	0.966	0.968	0.976	0.989	1.008	1.025	1.028	1.016	0.997	0.987	0.990
5.00	1.022	1.023	1.026	1.029	1.026	1.017	1.003	0.990	0.986	0.992	1.002

nature of the superposition approximation. The error apparent for nearly linear configurations at the higher density is due to the finite size of the mesh (see the appendix of Ref. 13). Comparing the two figures suggests that the approximation is better in absolute terms at the lower density, at least for the fluid phase considered here. This is in agreement with the extensive results of Krumhansl and Wang[13] for a Lennard-Jones fluid, but not with the conclusion of Alder,[11] perhaps because of the few configurations examined in the latter study. One would have thought that the independent probability assumption which underlies the superposition to have a larger range of validity at low densities. It is straightforward to obtain the triplet direct correlation function from the three particle distribution function discussed above, via the Fourier transformed triplet Ornstein–Zernike equation (Ref. 34, for example).

IV. CONCLUSION

In this paper a general method has been given for treating spherically inhomogeneous systems with integral equation theories. The full inhomogeneous pair correlation functions are available from the procedure. That the approach is practical was demonstrated by the results obtained for a hard-sphere fluid. Those data were more accurate than when the same pair closure is used in the usual bulk formulation of the problem, evidently because the approximation is being

TABLE VI. Same as Table IV but with $\mathbf{r}_1 = (0,3)$.

	0.00	0.25	0.50	0.75	1.00	1.25	1.50	1.75	2.00	2.25	2.50
0.00	...	...	...	...	0.957	1.071	1.002	1.001	0.955	0.996	1.008
0.25	...	...	...	...	0.941	1.090	1.029	1.021	0.964	0.995	0.998
0.50	...	...	...	...	0.974	0.999	1.019	1.025	0.992	1.012	0.994
0.75	...	...	...	0.980	1.007	0.933	0.977	0.995	1.008	1.031	1.008
1.00	0.958	1.011	1.133	1.172	1.077	0.996	0.979	0.938	0.981	1.027	1.028
1.25	0.808	0.838	0.882	0.956	1.090	1.133	1.049	0.962	0.951	0.988	1.032
1.50	0.782	0.778	0.778	0.784	0.856	1.018	1.136	1.051	0.955	0.954	1.006
1.75	1.307	1.245	1.054	0.860	0.770	0.837	1.034	1.127	1.014	0.948	0.978
2.00	2.816	2.616	2.017	1.370	0.921	0.770	0.879	1.094	1.083	0.972	0.958
2.25	0.000	0.000	0.000	2.451	1.383	0.856	0.806	0.974	1.120	1.012	0.952
2.50	0.000	0.000	0.000	0.000	2.075	1.078	0.801	0.877	1.106	1.052	0.957
2.75	0.000	0.000	0.000	0.000	2.676	1.320	0.816	0.839	1.070	1.076	0.964
3.00	0.000	0.000	0.000	0.000	3.000	1.399	0.831	0.830	1.062	1.080	0.966
3.25	0.000	0.000	0.000	0.000	2.703	1.323	0.824	0.839	1.089	1.073	0.959
3.50	0.000	0.000	0.000	0.000	2.099	1.082	0.777	0.882	1.108	1.051	0.953
3.75	0.000	0.000	0.000	2.453	1.390	0.880	0.800	0.973	1.118	1.051	0.951
4.00	2.827	2.631	2.028	1.359	0.921	0.780	0.872	1.082	1.090	0.971	0.952
4.25	1.322	1.252	1.049	0.857	0.783	0.849	1.029	1.122	1.017	0.951	0.975
4.50	0.812	0.801	0.775	0.790	0.875	1.029	1.126	1.046	0.961	0.956	1.004
4.75	0.827	0.836	0.879	0.974	1.098	1.126	1.045	0.964	0.950	0.989	1.024
5.00	1.107	1.114	1.136	1.136	1.087	1.013	0.957	0.951	0.984	1.021	1.023

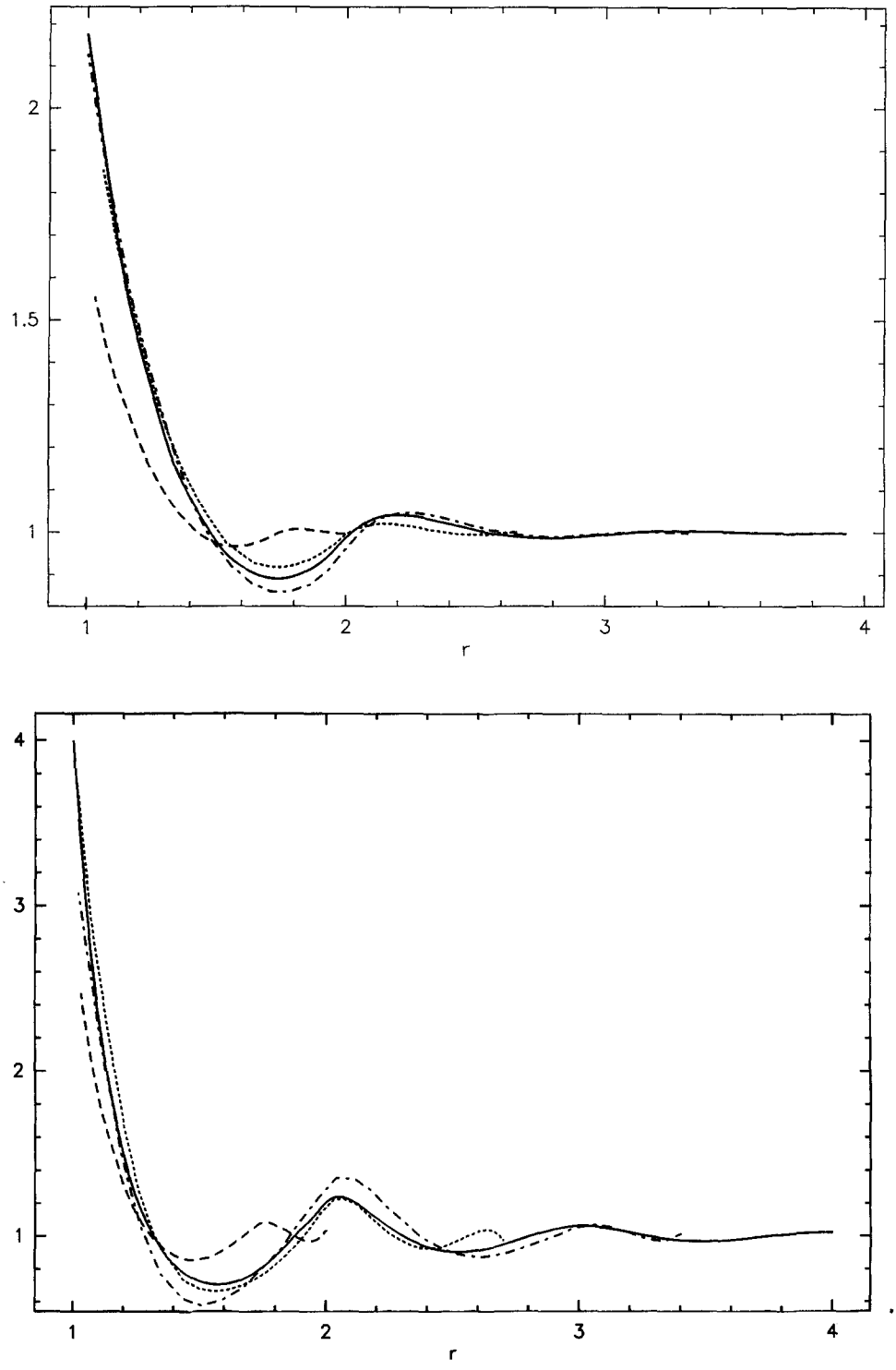

FIG. 3. (a) The inhomogeneous pair correlation function $g_0(\mathbf{r}_1,\mathbf{r}_2)$ for $\mathbf{r}_1 = \mathbf{r}_2 = s$ as a function of $r_{12} = r$, compared to the PY3 radial distribution function $g(r)$ (solid line). The long dashes, short dashes and long/short dashes correspond to $s = 1$, 1.33, and 1.67, respectively. The density is $\rho d^3 = 0.5$. (b) Same as the preceding figure but for $\rho d^3 = 0.8$

applied at a higher level in the hierarchy of distribution functions. A good example of this effect is the Debye–Hückel theory for bulk electrolytes. This uses a mean-field linearized Poisson–Boltzmann approach, but in the presence of an ion. This is an advance on treating the bulk simply as an ideal gas, and is equivalent to describing the bulk problem at the pair level, using the mean spherical approximation (MSA) closure. The formalism introduced in this paper allows application of this principle to more general fluids and arbritary closures, and at a further level (the triplet level) in the hierarchy.

Treating the inhomogeneous fluid at the two-particle level is equivalent to describing a three-body interaction, the fixed particle (or the wall for planar inhomogeneous problems) being the third member of the trio. Yet because the correlations go over to the bulk pair correlations away from the fixed particle, it is essential to go to this triplet level in order to achieve a pair with the usual two-particle results for bulk fluids. Again Debye–Hückel provides a fecund example. Compare that two-particle theory of the bulk with the linearised Poisson–Boltzmann approach to the electric double layer. The latter is well known as a mean-field approxi-

mation, and yet it is equivalent to also invoking the MSA closure, but for the wall–atom and bulk atom–atom direct correlation functions in the singlet integral equation approach. On the other hand, applying the same closure to the inhomogeneous pair correlation functions themselves gives a substantial improvement on Poisson–Boltzmann theory.[7] It is the level at which the closure approximation is applied which ultimately limits the utility of the singlet theories for planar inhomogeneous fluids (and also treatments of highly asymmetric bulk mixtures).

To accurately describe the fluid around a spherical particle, and thence the interactions between particles, are important problems. Much experience and expertise has been gained with integral equation theories for the bulk. The procedures given in this paper enable these techniques to be applied to spherically inhomogeneous fluids.

APPENDIX: NUMERICAL PROCEDURES

The discrete Legendre transform, Eqs. (12) and (13), requires nodes, weights, and the value of the Legendre polynomials. These may be found by the usual recurrance relationships (see Sec. 4.5 of Ref. 32). In working with any transform it is desirable to use continuous functions. Thus while the function $\hat{y}=\hat{h}-\hat{c}$ is suitable, the direct correlation function itself is discontinuous across the hard core. If this is transformed directly then the location of the core becomes lost (there is an uncertainty of the order of the mesh), and long-range tails also occur in the transform. The discontinuities need to be subtracted and transformed analytically.

Define $a\equiv c(x_d^-)$ and $b\equiv c'(x_d^-)$ to be the values of the direct correlation function and its first derivative just inside angular contact of two atoms x_d. One requires the Legendre transform of

$$f(x)=\begin{cases}0, & -1\leqslant x<x_d\\ a+b(x-x_d), & x_d\leqslant x\leqslant 1\end{cases}, \tag{A1}$$

and this is

$$\hat{f}_n=(a-bx_d)(1-x_d)\frac{2n+1}{2n}[x_dP_n(x_d)-P_{n+1}(x_d)]+\frac{b}{2}\left\{\left[\frac{2n+1}{n-1}x_d^2-\frac{2n+1}{(n-1)(n+2)}\right]\right.$$
$$\left.\times P_n(x_d)-x_d\frac{(2n+1)(n+1)}{(n-1)(n+2)}P_{n+1}(x_d)\right\}, \tag{A2}$$

for $n\geqslant 2$, and

$$\hat{f}_0=(a-bx_d)(1-x_d)/2+b(1-x_d^2)/4$$
$$\hat{f}_1=3(a-bx_d)(1-x_d^2)/4+b(1-x_d^3)/2$$

otherwise. Hence the continuous function $c^c\equiv c-f$ may be readily numerically transformed, and the desired transform of the direct correlation function is $\hat{c}_n=\hat{c}_n^c+\hat{f}_n$.

The Ornstein–Zernike equation (11) has to be truncated and discretized. One should take the fluid to be bulk beyond some large cutoff, and this is particularly easy to implement with the PY closure for hard spheres, by approximating $\hat{Y}_n$ close to the boundary by its bulk value. That is, combine the exact (within the PY closure) relationship

$$\hat{y}_n(r_i,r_j)=\frac{4\pi}{2n+1}\int_S^R dr_3\, r_3^2\hat{c}_n(r_i,r_3)\rho(r_3)\hat{h}_n(r_3,r_j), \tag{A3}$$

for $S<r_i\leqslant r_j<R-d$, with the approximation

$$\hat{y}_n(r_i,r_j)=\hat{y}_n^{\infty}(r_i,r_j)\,, \tag{A4}$$

for $R-d\leqslant r_i\leqslant r_j\leqslant R$. The analytic expressions for the PY bulk pair correlation functions[27,28] were used, and the results were indistinguishable from those obtained using self-consistent bulk pair correlations. In practice, the effects of the bulk approximation can be minimized by always choosing $r_i\leqslant r_j$ since there are relatively few pairs such that $r_j\geqslant r_i\geqslant R-d$, and these are the only ones which contribute to the above. A choice is available because the correlation functions are symmetric in their arguments. The functions were discretized on a uniformly spaced radial mesh and the integral evaluated using the trapezoidal rule.

The heart of the computational algorithm begins with $\hat{Y}$, either from the last iteration, from a restart file, or from Legendre transforms of the analytic solution to the PY equation for bulk hard-spheres. This is inverse Legendre transformed and the matrix of direct correlation functions C extracted, via the PY closure. This matrix is made continuous, transformed back to Legendre space, and the analytic transform of the discontinuities are added. From this $\hat{C}$ and the old $\hat{Y}$ a new $\hat{H}$ is assembled. This is used in generating a new profile ρ, by Eq. (25). Then the profile, $\hat{H}$, and $\hat{C}$ are used to create a new $\hat{Y}$ by the Ornstein–Zernike equation. The iteration repeats until satisfactory convergence is achieved.

Most of the results reported in the text were obtained with up to 60 mesh points in the angular direction (nodes), and 120 in the radial direction, with a bulk cutoff $R=9$. Reducing the radial mesh cutoff by 30% decreased the virial osmotic coefficient by 0.1% at $\rho d^3=0.75$. Increasing the number of layers per diameter from 15 to 20 (consequently reducing R to 7) increased ϕ_v by about 2% to 7.70 at $\rho d^3=0.80$. The results were much less sensitive to the angular mesh, but the compressibility was greatly affected by reducing the bulk cutoff at these densities. The calculations were performed on a VAX 8600, with each iteration requiring about 1 min of CPU time. To achieve four-figure convergence in the osmotic coefficient several hundred iterations were required at higher densities where a mixing fraction of the order of 10% was used.

[1]S. Sokolowski, J. Chem. Phys. **73**, 3507 (1980).
[2]R. M. Nieminen and N. W. Ashcroft, Phys. Rev. A **24**, 560 (1981).
[3]B. Borstnick and D. Janezic, Mol. Phys. **50**, 1199 (1983).
[4]R. Kjellander and S. Marčelja, J. Chem. Phys. **82**, 2122 (1985).

[5]R. A. McGough and M. D. Miller, Phys. Rev. A **34**, 457 (1986).
[6]M. Plischke and D. Henderson, J. Chem. Phys. **84**, 2846 (1986).
[7]P. Attard, D. J. Mitchell, and B. W. Ninham, J. Chem. Phys. **88**, 4987 (1988).
[8]E. Bruno and C. Caccamo, Phys. Rev. A **38**, 515 (1988).
[9]P. A. Egelstaff, D. I. Page, and C. R. T. Heard, Phys. Lett. A **30**, 376 (1969).
[10]H. J. Raveché and R. D. Mountain, J. Chem. Phys. **53**, 3101 (1970).
[11]B. J. Alder, Phys. Rev. Lett. **12**, 317 (1964).
[12]A. Rahman, Phys. Rev. Lett. **12**, 575 (1964).
[13]J. A. Krumhansl and S. S. Wang, J. Chem. Phys. **56**, 2034 (1972).
[14]J. G. Kirkwood, J. Chem. Phys. **3**, 300 (1935).
[15]H. W. Jackson and E. Feenberg, Rev. Mod. Phys. **34**, 686 (1962).
[16]S. Ichimaru, Phys. Rev. A **2**, 494 (1970).
[17]A. D. J. Haymet, S. A. Rice, and W. G. Madden, J. Chem. Phys. **74**, 3033 (1981).
[18]J. L. Barrat, J. P. Hansen, and G. Pastore, Phys. Rev. Lett. **58**, 2075 (1987).
[19]G. Arfken, *Mathematical Methods for Physicists* (Academic, New York, 1970).
[20]M. Abramowitz and I. A. Stegun, *Handbook of Mathematical Functions* (Dover, New York, 1965).
[21]D. G. Triezenberg and R. Zwanzwig, Phys. Rev. Lett. **28**, 1183 (1972).
[22]R. A. Lovett, C. Y. Mou, and F. P. Buff, J. Chem. Phys. **58**, 1880 (1976).
[23]M. S. Wertheim, J. Chem. Phys. **65**, 2377 (1976).
[24]M. Born and H. S. Green, Proc. R. Soc. London Ser. A **188**, 10 (1946).
[25]J. Yvon, *La Théorie Statistique des Fluides et L'Equation de'État Act.* (Sci. Ind. Hermann, 1935), Vol. 203.
[26]N. N. Bogoliubov, J. Phys. (Moscow) **10**, 256 (1946).
[27]E. Thiele, J. Chem. Phys. **39**, 474 (1963).
[28]M. S. Wertheim, Phys. Rev. Lett. **10**, 321 (1963).
[29]S. Sokolowski, Mol. Phys. **49**, 1481 (1983).
[30]M. Plischke and D. Henderson, Proc. R. Soc. London Ser. A **404**, 323 (1986).
[31]R. Kjellander and S. Sarmen, Chem. Phys. Lett. **149**, 102 (1988).
[32]W. H. Press, B. P. Flannery, S. A. Teukolsky, and W. T. Vetterling, *Numerical Recipes. The Art of Scientific Computing* (Cambridge, New York, 1986).
[33]N. Carnahan and K. Starling, J. Chem. Phys. **53**, 600 (1970).
[34]J. A. Barker and D. Henderson, Mol. Phys. **21**, 187 (1971).
[35]B. J. Alder, and C. E. Hecht, J. Chem. Phys. **50**, 2032 (1969).